# Ulvan/Silver nanoparticle hydrogel films for burn wound dressing

Evi Sulastri [a,c], Ronny Lesmana [b], Muhammad Sulaiman Zubair [c],
Ahmed Fouad Abdelwahab Mohammed [d], Khaled M. Elamin [e], Nasrul Wathoni [a,*]

[a] *Department of Pharmaceutics and Pharmaceutical Technology, Faculty of Pharmacy, Universitas Padjadjaran, Sumedang, 45363, Indonesia*
[b] *Department of Anatomy, Physiology and Biology Cell, Faculty of Medicine, Universitas Padjadjaran, Sumedang, 45363, Indonesia*
[c] *Department of Pharmacy, Faculty of Mathematics and Natural Sciences, Universitas Tadulako, Palu, 94119, Indonesia*
[d] *Department of Pharmaceutics, Faculty of Pharmacy, Minia University, Minia, 61519, Egypt*
[e] *Graduate School of Pharmaceutical Sciences, Kumamoto University, 5-1 Oe-honmachi, Chuo-ku, Kumamoto, 862-0973, Japan*

A R T I C L E   I N F O

A B S T R A C T

Ulvan is a polysaccharide from green algae that shows good hydrogel film dressing characteristics. Silver nanoparticles (AgNP) can be incorporated into the hydrogel film to improve antibacterial properties and provide a potential burn treatment. In this study, we developed a novel hydrogel film wound dressing composed of ulvan and silver nanoparticles. Two concentrations (0.5 mM and 1 mM) of silver nitrate were used to produce ulvan-silver nanoparticles hydrogel film (UHF–AgNP0.5 and UHF–AgNP1), respectively. The physicochemical characteristics of the hydrogel films were evaluated, including particle size, zeta potential, Fourier transform infrared (FTIR), X-ray diffractometry (XRD), scanning electron microscope and energy-dispersive X-ray (SEM-EDX). Furthermore, the in vitro antimicrobial activity, and second-degree burn wound healing test were evaluated. The UHF–AgNP0.5 showed the highest antimicrobial activity compared to UHF–AgNP1 and UHF film. Meanwhile, an in vivo study using Wistar rats induced second-degree burns showed that UHF–AgNP0.5 significantly accelerated the healing process by regulating the inflammatory process, increasing re-epithelialization, and improving the vascularization process. Ulvan-silver nanoparticle hydrogel films have the ability to accelerate the healing of second-degree burns and are potential candidates for wound dressings.

## 1. Introduction

Burns is a significant health problem that causes about 180.000 deaths every year, especially in poor and developing countries [1]. The high cost of treatment in handling cases of burns is also an essential part of the urgency to find a cost-effective treatment method. For instance, the total cost of treating burn patients in low to middle-income countries is 5.196 USD and 88.218 USD in high-income countries. This figure is higher than trauma and surgery patients [2]. Meanwhile, the biggest cost in treating burns is the use of antibiotics [3]. Various technologies are applied in wound treatment efforts to produce more precise, effective, and efficient treatment management. Research has shown that treating wounds conditioned in a closed and moist condition results in faster re-epithelialization and increased cell migration, leading to accelerated healing, compared to damages in open and dry conditions [4, 5]. Optimal burn treatment could be achieved by utilizing biologically active materials that have a significant role in wound healing, such as antimicrobial agents.

---

Our previous research showed that ulvan hydrogel films have moderate activity against bacteria *Staphylococcus aureus*, *Staphylococcus epidermidis*, *Escherichia coli*, and *Pseudomonas aeruginosa* [6]. Ibrahim et al. [7] reported the antimicrobial activity of ulvan against gram-positive pathogenic microbial strains, *Bacillus subtilis*, and *Staphylococcus epidermidis*, and gram-negative strains are *Aeromonas hydrophila*, *Pseudomonas fluorescens*, *Pseudomonas aeruginosa*, *Escherichia coli*, and *Klebsiella pneumoniae*, as well as fungal strain is *Candida albicans*. Ulvan is a water-soluble sulfate polysaccharide from green algae (*Chlorophyta*). The main constituent of Its structure is sulfated rhamnose bound to uronic acid via 1,4-glycosidic bonds [8]. Silver nanoparticles (AgNPs) are one of the most fascinating metallic nanomaterials, having multiple applications in the biomedical field. Silver products have been explored for centuries to prevent and treat various diseases, especially infections, due to their potent inhibition against microbes such as *Escherichia coli*, *Staphylococcus aureus*, and anti-fungal activity against *Trichosporon beigelii* and *Candida albicans* [9]. The antimicrobial properties of silver depend on the amount of silver in the formula and the release of silver. Silver ions are highly reactive, attach to tissue proteins, cause structural changes in the bacterial cell wall and nuclear membrane, and ultimately cause cell deformation and death. The physicochemical characteristics, particle size, morphology, and stability of nanoparticles are essential in this application. The size and shape of the nanoparticles can be controlled by optimizing the reaction parameters such as pH, temperature, metal solution concentration, and reducing agent concentration [10].

Interestingly, silver can be synthesized biologically, known through green synthesis technology, using plants and bacteria. This technology utilizes material or plant content as a reducing agent (bioreactor). Several bioreactors have been investigated, including antioxidant compounds, chitosan, alginate, and others have been explored. Massironi et al. [11] have carried out a green synthesis of AgNP using ulvan as a reducing agent with increased stability.

Several previous researchers have investigated the production of wound dressings with polymers and AgNPs. Diniz et al. [12] prepared a hydrogel dressing from sodium alginate and gelatin. Meanwhile, the fabrication of burn dressings from carrageenan/alginate/AgNPs was carried out by Zia et al. [13]. The cellulose nanocrystals from *Dendrocalamus hamiltonii* and *Bambusa bambos* leaves were successfully used to develop biomaterial nanocomposite dressing that significantly enhances skin tissue repair and accelerates wound healing [14]. A composite of Konjac glucomannan and AgNPs was also successfully prepared with antimicrobial capacity and showed accelerated wound healing time [15]. Likewise, the chitosan could stabilize AgNPs in film dressing and showed good antimicrobial activity, making it a good candidate for wound dressing [16]. Thus, in this study we developed AgNPs on Ulvan film dressings and evaluated the antimicrobial and wound dressing properties. As well as their in vivo wound healing activity using Wistar rats. The AgNPs are synthesized by in situ method, which ulvan at the same time was used as the reducing agent.

## 2. Material and methods

### 2.1. Materials

Ulvan was extracted from green algae *Ulva Lactuca* Linn., ethanol, boric acid, glycerol, deionized water, phosphate-buffered saline (PBS) media, silver nitrate, anhydrous calcium chloride, silver nitrate (AgNO$_3$), Mueller Hinton Agar (MHA) were purchased from Sigma-Aldrich. Star® Ag gel, *Escherichia coli* (*E. coli*, ATCC® 35281), *Staphylococcus aureus* (*S. aureus*, ATCC® 25923), and *Pseudomonas aeruginosa* (*P. aeruginosa*, ATCC® 9027), *Staphylococcus epidermidis* (*S. epidermidis*, ATCC® 12228) were purchased from Microbiologics.

### 2.2. Preparation of UHF–AgNP

The ulvan hydrogel was prepared according to the procedure in the previous study [5], while the AgNPs formation was performed by in situ method which is no external reducing and stabilizing agent were added [17]. AgNO$_3$ concentration of 0.5 mM and 1 mM was prepared in deionized water. Then, each AgNO$_3$ solution was added to the hydrogel at room temperature, stirred at 300 rpm for 40 min, and sonicated for 20 min. The formation of Ag nanoparticles is characterized by a change in the color of the solution mixture from yellowish green to brownish orange [18]. The hydrogel was dried at 45 °C for 48 h to obtain UHF–AgNP0.5 and UHF–AgNP1. In this study, the Ulvan hydrogel film (UHF) was also produced [6] as a control test (antimicrobial and in vivo analysis).

### 2.3. Evaluation of UHF–AgNP

#### 2.3.1. Physical characteristics

The pH was determined by a pH meter. One percent of each sample was diluted with distilled water (20.0 mL) in a glass beaker (25.0 mL). The pH should be in the range of 4.5–6.5. The viscosity of samples was determined by a viscometer (Brookfield). The sample weights were measured using an analytical balance, and the thicknesses were measured using Vernier calipers. Meanwhile, the swelling degree test analysis was performed by immersing the sample (1.5 × 1.5 cm) in phosphate buffer saline solution (25 mL) at pH 7.4 (room temperature). After 1, 4, and 6 h, the sample was slowly removed from the buffer solution, and the excess buffer on the surface of the sample was dried with filter paper, and then the sample was reweighed. The measurement was repeated at five different film positions with 0.001 mm accuracy. The following equation was used to calculate the swelling degree:

$$\% \text{ Swelling degree} = (Ws - Wd)/Wd \times 100 \tag{1}$$

where Ws is the weight of swollen film at a certain time, and Wd is the weight of the first film (dried film).

For the water vapor transmission rate (WVTR) test, a five g anhydrous calcium chloride was placed into a weighted bottle. The sample was fixed and laid on the top of the bottle and tied with thread; then, the vial was placed into a desiccator (75% RH at room temperature). The sample WVTR is calculated according to the following equation:

$$WVTR = W/S \tag{2}$$

where W represents the weight of the film at 24 h, and S represents the area of the film ($m^2$).

### 2.3.2. UV-VIS spectrophotometer analysis

UV-VIS absorption spectra were analyzed using a UV–Vis spectrophotometer (*Cecil*®) in the scanning range of 300–700 nm. All samples were run at room temperature.

### 2.3.3. Particle size and zeta potential analysis

The zeta potential of AgNPs was measured by dynamic light scattering (Malvern Zetasizer Instrument). This analysis can measure the zeta potential in diluted aqueous samples of UHF-AgNPs hydrogel film. TEM (JEM-1400) was used to investigate the particle size of AgNPs. The instrument was operated at 120 kV to capture the image of the sample. Then, the particle size of the AgNPs was measured using ImageJ® software.

### 2.3.4. Fourier transform infrared (FTIR) spectroscopy

FTIR spectra of UHF and UHF-AgNPs samples were recorded by IR Prestige-21 (Shimadzu®, Japan). All the samples were ground with potassium bromide in the ratio of 1:100 and made into a pellet. Analysis was performed at a range of frequencies from 4000 to 400 $cm^{-1}$ with a resolution of 4.0 $cm^{-1}$.

### 2.3.5. Scanning electron microscope and energy-dispersive X-ray spectroscopy (SEM-EDX)

SEM-EDX instrument by a Phenom Desktop ProXL was used to investigate the morphologies of AgNPs at an accelerating voltage was 15.00 kV. The SEM instrument is equipped with EDX to analyze the elemental composition.

### 2.3.6. XRD analysis

The XRD pattern of the AgNPs was investigated using a Bruker D2 Phaser instrument with Cu κα 1.54 Å radiation. The XRD spectra were recorded in the range 2θ from 10.0 to 70.0 with a stepwise increment of 0.02° and a count time of 5 s.

### 2.3.7. Antibacterial activity studies

The antibacterial capabilities of the AgNPs were determined using the agar well diffusion method against the positive strain bacterial *S. epidermidis*, and *S. aureus*. Also, the negative strain bacterial *E. coli* and *P. aeruginosa*. Mueller Hinton Agar (MHA) was heated at 121 °C for 15 min and then 20 mL of media was poured into sterile Petri dishes. The bacteria were added to the media and then allowed to solidify. After solidification, the puncture apparatus (inner diameter: 8 mm, outer diameter: 10 mm) was used to create the well. Then, 50 μL of the sample (UHF, UHF–AgNP0.5, and UHF–AgNP1) was poured into the well for the test. The Petri dish was then incubated at 37 °C for 24 h. Finally, the inhibition zone was measured using a sliding caliper in four directions and the average was determined. Three parallel samples were used in each experiment.

### 2.3.8. Wound healing studies

The experimental procedures were conducted as approved by the Ethical Committee of the Medical Faculty of Universitas Padjadjaran (Document approval number: 864/UN6.KEP/EC/2021). Experimental animals (male Wistar rats, weight (250–300 g) received intramuscular (i.m.) injections of ketamine (90 mg/kg BW). After the rats were properly anesthetized, trichotomy of the back. Second-degree thermal burns were made on the rat's skin with an area of 2 $cm^2$ at 170 °C for 15 s using a metal plate integrated with an automatic thermometer [19]. For every treatment, the plate is controlled so that the temperature remains the same. The wound was then cleaned with a sterile saline solution. Afterward, the rats were given paracetamol injection (0.5 mL) i.m. for three days to reduce pain. The rats were divided into four groups (negative control, positive control, UHF, UHF–AgNP), with each group consisting of six rats (n = 6, a total of 24 animals). The wound was covered with the dressing while the wound in the control group was left untreated. After receiving the treatment, each animal was housed and given ad libitum food. The dressing (2.5 $cm^2$) was changed once every two days in the wound area for 21 days. Each animal's wounds were observed and documented on days 0, 5, 7, 14, and 21 days after treatment. The following equation was used to calculate the percentage of wound closure rate:

$$\% \text{ Wound closure rate} : Sn / So \times 100 \tag{3}$$

where So is the initial wound area, and Sn is the wound area at a certain measurement time.

### 2.3.9. Histological analysis

This test was conducted to observe the compatibility of the wound dressing against the tissue. On days 1 and 21, rats for each treatment were sacrificed, and the wound area and surrounding tissue (0.5 cm) were carefully cut, washed in PBS solution, and then treated with 4% paraformaldehyde (PFA). The sample was dehydrated in stages with ethanol (70–100%), immersed in paraffin, and sliced 5 μm thick using a microtome (sections). Sections were stained with hematoxylin and eosin (H&E). The structures were observed

under a light microscope for histopathological changes.

## 2.4. Statistical analysis

The data were presented as a mean of ±SD for each experiment. The statistical analysis of the data was performed using the one-way analysis of variance (ANOVA) and comparisons between groups means through Tukey's test. The statistical significance was considered for a $p < 0.05$.

## 3. Results

### 3.1. Physical characteristics

Both UHF and UHF-AgNPs were brownish in color. While the pH of the two preparations was 7.09–7.43 with viscosity values of 367 and 356.9 cps. Thickness was 0.73 and 0.78, with 1.15 g and 1.27 g of weight for the UHF–AgNP0.5 and UHF–AgNP1 formulas, respectively (Table 1). This value is not too different from the previous study of ulvan hydrogel films [6]. Likewise, the value of the swelling degree and WVTR, which can be seen in Table 2, did not differ significantly from the results of UHF in previous studies, which could mean that the addition of AgNP to the UHF did not affect these characteristics.

### 3.2. Ultraviolet–visible study

In this study, the addition of $AgNO_3$ precursor in hydrogel Ulvan produce a change in the color from yellowish green to brownish caused by reduction of pure Ag(I) ions to Ag (0). Fig. 1 shows, the absorbance of AgNPs was read at the maximum wavelength of 400.4 nm and 411.86 nm (for UHF–AgNP0.5 and UHF–AgNP1).

### 3.3. Particle size and zeta potential

The result of the size and zeta potential of the UHF–AgNP film displayed in Fig. 2 and Table 3. The results showed particle sizes of ~13.87–21.55 nm and ~22.44–34.77 nm for UHF–AgNP0.5 and UHF–AgNP1, respectively. Meanwhile, the morphology of AgNPs is mostly spherical by the TEM instrument. The zeta potential index values ($-24.5 \pm 1.47$ and $-22.43 \pm 2.5$) of the two formulas were in a good range to maintain the stability of the preparation during storage even though a higher value is still expected to maintain the stability of the hydrogel film preparation for a more extended period of time.

### 3.4. FTIR spectroscopy

The FTIR spectra of UHF–AgNP0.5 and UHF–AgNP1 are displayed in Fig. 3a. The ulvan peaks at UHF–AgNP0.5 and UHF–AgNP1 are characteristic of the carboxyl groups of uronic acid [20,21] and exhibit two characteristic signals of C=O: one for a symmetrical stretch at 1631 $cm^{-1}$ in both formulas for and an asymmetrical stretch at 1431 $cm^{-1}$ (UHF–AgNP0.5) and 1433 $cm^{-1}$ (UHF–AgNP1). Moreover, the peak at 848 $cm^{-1}$ is for C–O–S, a characteristic glycoside bond in the Ulvan structure, indicating the presence of polysaccharides. The peaks at 1253 $cm^{-1}$ and 1255 $cm^{-1}$ (in UHF–AgNP0.5 and UHF–AgNP1, respectively) correspond to the stretching of the S=O sulfate group. These functional groups are generally abundant in the ulvan structure [22,23].

### 3.5. XRD analysis

As shown in Fig. 3b, Ulvan diffraction patterns were seen in both UHF-AgNPs at peaks 31.308 and 31.300 for UHFAgNP0.5 and UHF–AgNP1 respectively. This result resembles the ulvan diffraction pattern in the previous study [6]. A diffraction peak at 2θ with values of 45,047; 56,076 and 65,933 for UHF–AgNP0.5. Meanwhile, diffraction peak at 2θ = 44,998; 56,096 and 65,864 for UHF–AgNP1. These peaks correspond to the Miller plane (h k l) (111), (200), (220) which indicates that the resulting particles are silver nano-particles with FCC/face center cubic symmetry of Ag ions in ulvan hydrogel networks.

### 3.6. SEM-EDX analysis

SEM is an electron microscope that produces images by scanning the surface with a focused beam of electrons with magnification

**Table 1**
Weight, thickness, pH, and viscosity of UHF-AgNPs (mean ± SD, n = 3).

| Hydrogel Film | Weight (g) | Thickness (mm) | pH | Viscosity (Cps) |
|---|---|---|---|---|
| UHF–AgNP0.5 | 1.15 ± 0.05 | 0.73 ± 0.03 | 7.09 ± 0.14 | 367 ± 14.52 |
| UHF–AgNP1 | 1.27 ± 0.08 | 0.78 ± 0.07 | 7.43 ± 0.2 | 356.9 ± 34.8 |

UHF–AgNP0.5 = Ulvan-silver nanoparticles hydrogel film with 0.5 mM silver nitrate, UHF–AgNP1= Ulvan-silver nanoparticles hydrogel film with 1 mM silver nitrate.

**Table 2**
Degree of swelling and WVTR value of UHF-AgNPs (mean $\pm$ SD, n = 3).

| Hydrogel Film | Swelling Degree (%) | | | WVTR (g/m$^2$/day) |
|---|---|---|---|---|
| | 1 h | 4 h | 6 h | |
| UHF–AgNP0.5 | 91.3 $\pm$ 9.03 | 138 $\pm$ 9.85 | 149 $\pm$ 5.57 | 1732 $\pm$ 23 |
| UHF–AgNP1 | 89.4 $\pm$ 9.93 | 127.3 $\pm$ 6.66 | 138.5 $\pm$ 4.22 | 1809 $\pm$ 28 |
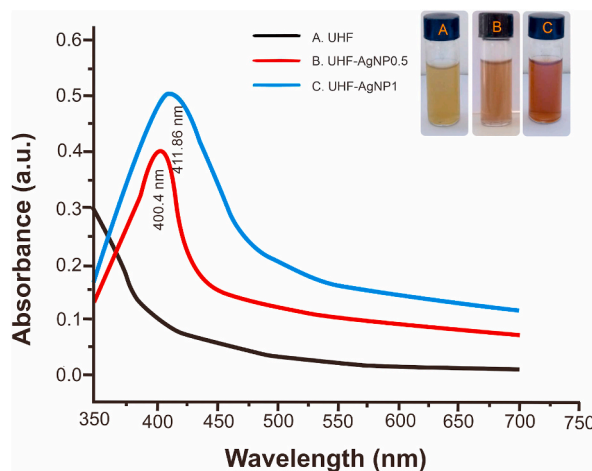


**Fig. 1.** UV–Vis absorption spectra of UHF, UHF–AgNP0.5, and UHF–AgNP1.
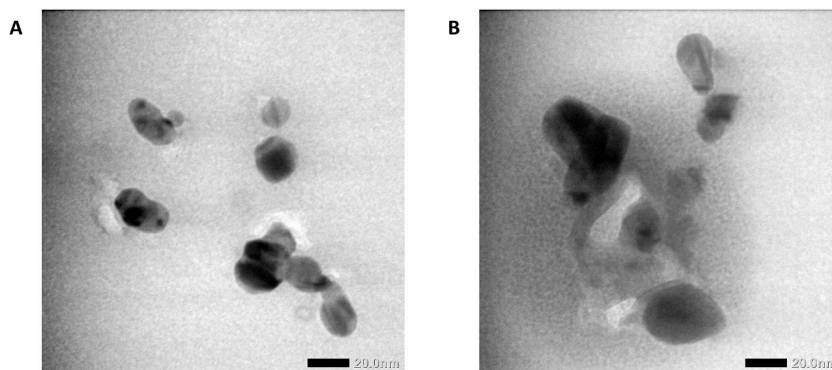


**Fig. 2.** TEM image of (a) UHF–AgNP0.5, and (b) UHF–AgNP1.

**Table 3**
The Zeta potential of UHF-AgNPs (mean $\pm$ SD, n = 3).

| Hydrogel Film | Zeta potential (mV) |
|---|---|
| UHF–AgNP0.5 | −24.5 $\pm$ 1.47 |
| UHF–AgNP1 | −22.43 $\pm$ 2.5 |

up to a particular scale. The electrons interact with the sample's atoms, producing various signals that contain information about the sample's surface topography. Meanwhile, the combination of this instrument with EDX is intended for the chemical elemental analysis of samples. This analytical capability is mainly due to the principle that each element has a unique atomic structure that allows for a unique collection of peaks in its electromagnetic emission spectrum. The sample's chemical composition percentage was obtained using the ZAF algorithm, where Z represents the element's atomic number, A represents the absorbance, and F represents the fluorescence value. Through this algorithm, the atomic percent and weight of the sample are obtained. As shown in Fig. 4a and b, the AgNPs morphology of some particles appeared quite spherical and tends to be flower-shaped, especially in UHF–AgNP1. The EDX spectra confirmed Ag presence in both film samples. Meanwhile, the mass percentage of silver was more significant in UHF–AgNP1 by
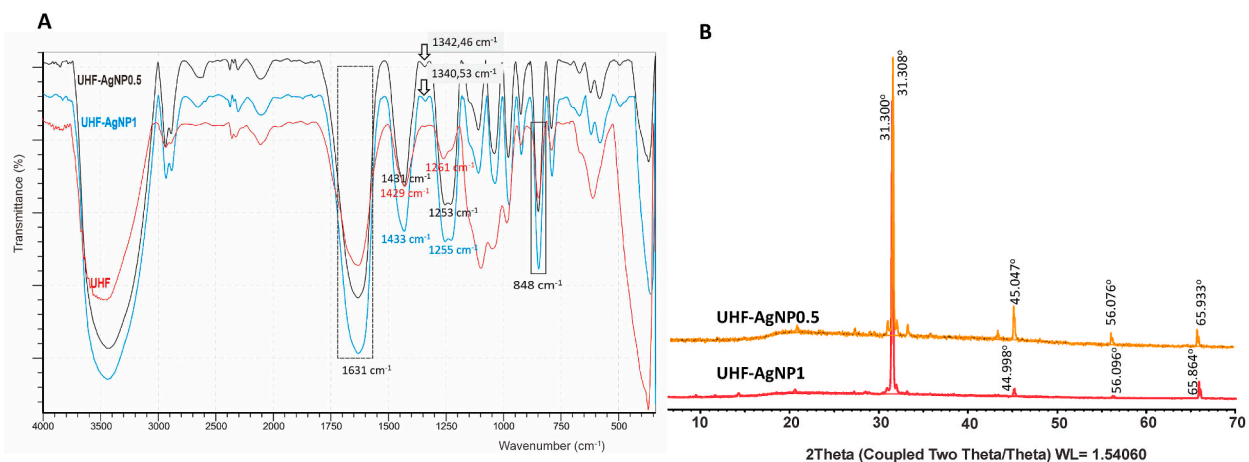
**Fig. 3.** (a) FTIR Spectra, and (b) XRD pattern of UHF–AgNP0.5, and UHF–AgNP1.

5.78% with an atomic percentage of 3.49% compared to UHF–AgNP0.5 at 3.92% with an atomic percentage of 2.97% (Fig. 4c and d). This is in line with the higher Ag concentration in UHF–AgNP1.

### 3.7. Antibacterial activity studies

The antimicrobial properties of the UHF, UHF–AgNP0.5 and UHF–AgNP1 hydrogel film formulas were tested against *S. epidermidis*, *E. coli*, *S. aureus*, and *P. aeruginosa* bacteria. The diameter of the inhibition zone of AgNP0.5 for all bacteria was larger than that of AgNP1 (Fig. 5a). The largest zone of inhibition was shown in *P. aeruginosa* bacteria, at 17.39 mm, then *S. aureus* at 17.35 mm, then *S. epidermidis* at 16.75 mm, and the last in *E. coli* at 13.58 mm for the UHF–AgNP0.5 formula. Meanwhile, UHF–AgNP1 was 13.07 mm, 15.36 mm, 14.89 mm, and 12.55 mm for *P. aeruginosa*, *S. aureus*, *S. epidermidis*, and *E. coli* bacteria, respectively. As shown in Fig. 5B, UHF–AgNP0.5 showed significant antibacterial activity than UHF–AgNP1 and therefore, it was chosen for the next in vivo study.
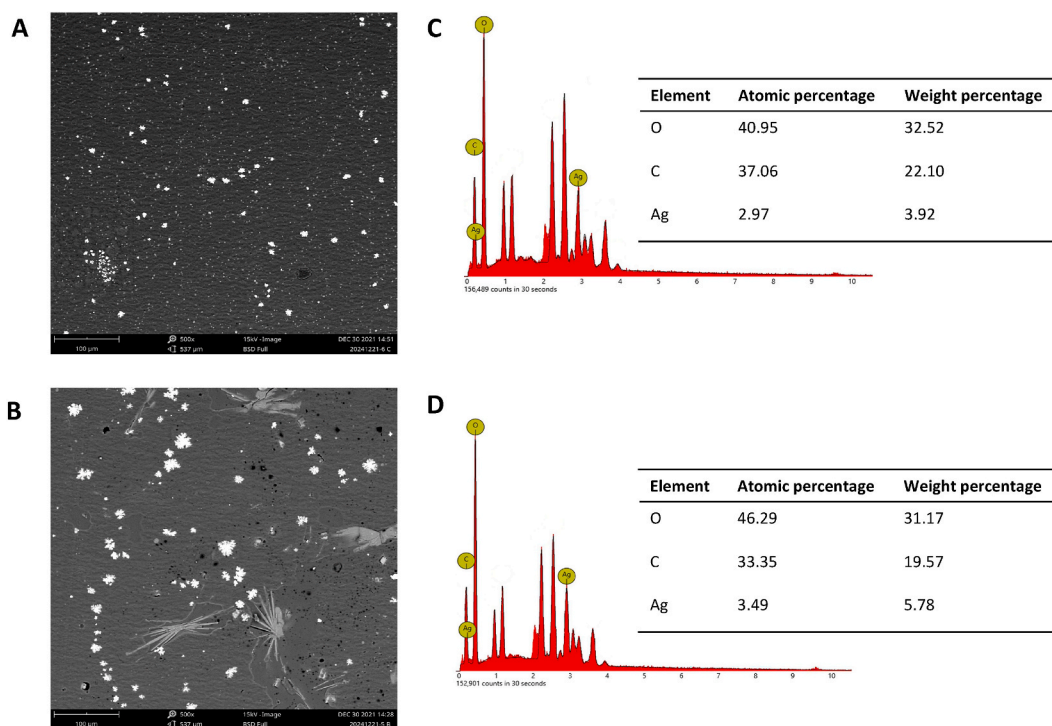


**Fig. 4.** Electron microscopy analysis of UHF–AgNP. (a) SEM images of UHF–AgNP0.5 at 500× magnification. (b) SEM images of UHF–AgNP1 at 500× magnification. (c) EDX of UHF–AgNP0.5 and (d) EDX of UHF–AgNP1.

**A**



**B**
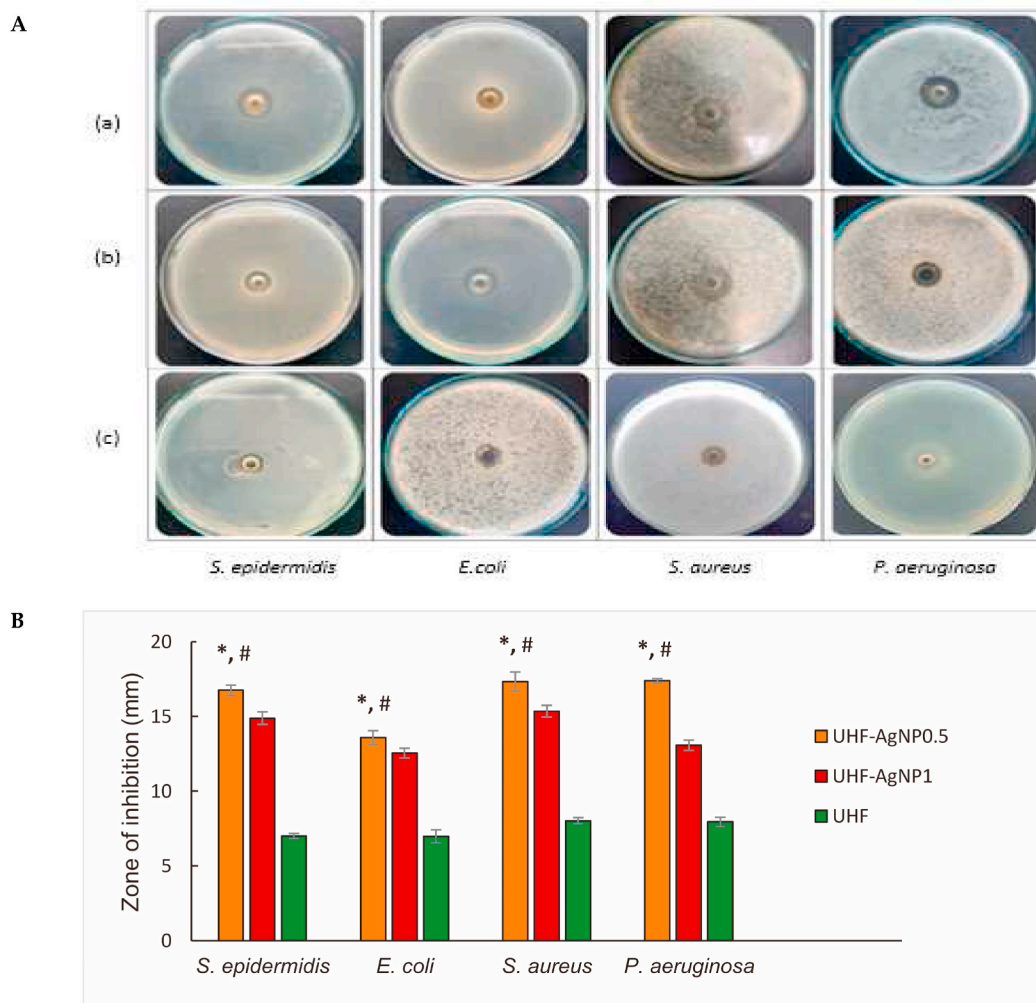


**Fig. 5.** A. (a). Antibacterial activities of a. UHF–AgNP0.5, (b). UHF–AgNP1, and (c). UHF against *S. epidermidis, E. coli, S. aureus, and P. aeruginosa*. B. The bar diagram represents the antibacterial studies of UHF–AgNP0.5, UHF–AgNP1, and UHF. Each value represents the mean ± SD of three experiments. *$p < 0.05$. UHF–AgNP0.5 compared to UHF–AgNP1. #$p < 0.05$, UHF–AgNP0.5 compared to the UHF.

### 3.8. Wound healing studies

In this study, UHF–AgNP0.5 was selected for in vivo activity testing because the evaluation results were more optimum than UHF–AgNP1. Furthermore, UHF–AgNP0.5 is simply called UHF–AgNP. Wound growth healing was noted on days 5, 7, 14, and 21 after infection (Fig. 6a and b). Each sample was applied to the wound on the first day after infection and thereafter every two days. On the fifth day after infection, wounds for UHF, UHF–AgNP, positive control, and negative control closed by 14.19%, 18.91%, 21.15%, and 9.26%, respectively. On the seventh day after infection, wound closure reached 43.89%, 61.39%, 62.26%, and 24.27%. In this phase, UHF–AgNP and positive control effectively reduced the wound area. On the 14th day after infection, significant wound closure occurred, namely 82.94%, 93.12%, 90.68%, and 41% for UHF, UHF–AgNP, positive control, and negative control respectively. At this stage, the percentage of wound healing almost tripled compared to day seven for the UHF–AgNP group and positive control. All wounds closed on day 21 except for the negative control group with a percentage of wound closure of 75.36%.

### 3.9. Histological analysis

In Fig. 6c, on day 1 after the burn induction treatment, the damage of the epidermis and partial loss of dermis in UHF, UHF–AgNP, positive control, and negative control indicate the occurrence of second-degree burns. Meanwhile, on day 21 of treatment, it was seen that UHF-AgNPs treated group showed the most significant improvement compared to UHF and negative control. Observations also showed improvements in positive controls resembling UHF–AgNP.
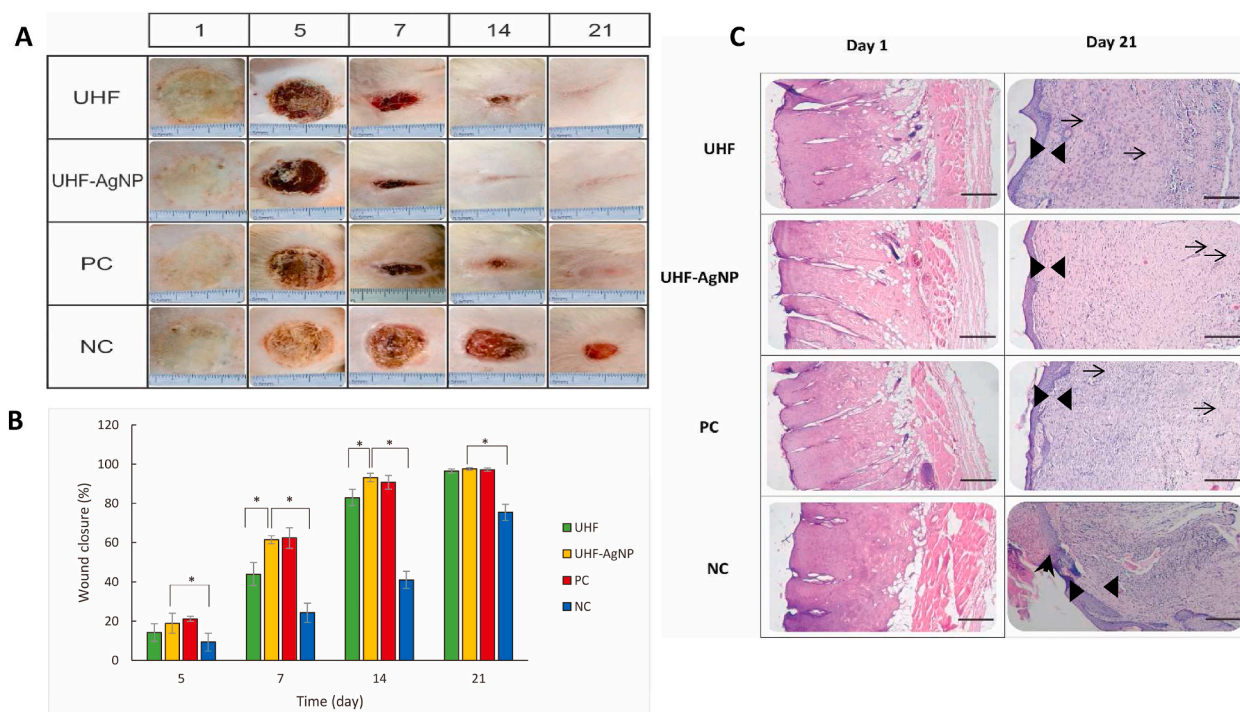
**Fig. 6.** A. Photomicrographs of second-degree wound assay on Wistar rats to evaluate the wound healing efficiency of UHF–AgNP. B. The bar diagram represents the wound reduction rate of UHF, UHF–AgNP, negative control NC, and PC. Each value represents the mean ± SD of three experiments. *p < 0.05. C. Micrographs image (Photograph with Olympus CX 33 photomicroscope 100× magnification) of H&E-stained tissue from burn wounds of UHF, UHF–AgNP, NC, and PC. The tissue between the black triangles is the epidermis, while the arrowhead is an un-epithelialized area, and the arrows are blood vessels that showed the presence of new vascular tissue in the newly regenerated dermis. Scale bar 100 μm.

## 4. Discussion

Burns are open wounds easily contaminated by bacteria. Thus, antibiotics are often used clinically for treatment. Therefore, the methods for treating burns topically vary widely, but how to control bacterial infection in wounds effectively is still a hot topic of discussion today. After a thermal burn, the skin barrier functions are damaged, causing various inflammations, and leading to bacterial infection. Modern medicine states that insufficient blood supply, edema, and necrosis after a burn event contribute to burn wound infection [24–26]. Multiple studies have reported the use of AgNPs as a new generation of non-antibiotic class antimicrobials with stable physical and chemical properties and strong broad-spectrum bactericidal capacity in recent years [27–29]. The strong permeability of AgNPs allows them to quickly penetrate the skin pores, killing various bacteria and fungi within minutes [27,30–32]. Likewise, the bacteria resistant to silver are rare, causing their wide biological application [30,33].

Silver nanoparticles are one of the most widely synthesized nano-metal preparations. Obtaining AgNPs was carried out by reducing $AgNO_3$ salts using inorganic reducing agents such as $NaBH_4$ and organic agents such as hydrazine. These chemicals are dangerous because of their relatively high toxicity and can be adsorbed on the material's surface. Green synthesis methods are becoming more and more popular for AgNP synthesis to overcome this problem [10,32,34]. The green synthesis of silver nanoparticles as antimicrobials has become one of the most researched areas of nanotechnology in recent years due to the numerous advantages it possesses, such as the utilization of natural resources, a relatively fast process, non-pathogenic procedures, low cost, and provides a simple technique for environmentally friendly biosynthetic processes [35]. Many researchers have reported a broad number of plants that facilitate the synthesis of silver nanoparticles, such as *Azadirachta indica* [36], *Urtica dioica* [37], *Calophyllum tomentosum* [38], *Berberis vulgaris* [10], *Gleichenia Pectinata* [39], polysaccharide from *Sanghuangporus sanghuang* [40], *Piper ningrum* seed [41], Arabinoglucan from *Lallemantia royleana* [42], *Mimosa tenuiflora* [43], *Moringa oleifera* seed polysaccharide [44], fucose-containing exopolysaccharide secreted by *Enterobacter* A47, FucoPol [45] and *Abelmoschus esculentus* [46].

The use of AgNPs against multidrug-resistant microorganisms resulted in superior antibacterial activity against Gram-negative multidrug-resistant (MDR) [18]. Another study using drug-resistant *P. aeruginosa* produced a significant antibacterial effect on antibiotic-resistant P. *aeruginosa* in a concentration and time-dependent manner [40]. Meanwhile, in the Naqvi et al. [47] study, it was reported that the combination of AgNPs with antibiotics produced a synergistic effect and could increase the efficacy of treatment against microbial pathogens.

In this recent study, the hydrogel film of ulvan optimization with the addition of $AgNO_3$ precursor to produce AgNPs showed the successful formation of AgNPs, which was characterized by a change in the color of the hydrogel from yellowish green to brownish.

UHF is used as the base in UHF10 which is the optimal concentration of ulvan in our previous studies based on the optimum characterization that has been carried out [6]. The absorbance of AgNPs was measured by UV-VIS spectrophotometry, and the absorbance was read at a maximum wavelength of 400.4 nm and 411.86 nm (for UHF–AgNP0.5 and UHF–AgNP1). It confirmed the silver nanoparticles formation in the hydrogel solutions is due to excitation of surface plasmon resonance (SPR) band of AgNPs [10,36]. At previous studies, the SPR peak of AgNPs located within 397–416 nm region [11]. For FTIR spectra, the results show an identical spectrum to UHF, which implies that the hydrogel film formulation did not break the main chain structure of ulvan. Additionally, the spectrum featured many peaks specific to this polysaccharide. The effectiveness of the UHF–AgNP formulation was indicated by the presence of new peaks at 1342 and 1340 cm$^{-1}$ for UHF–AgNP0.5 and UHF–AgNP1, respectively. This peak was not detected in the UHF and ulvan from the previous study [6]. These results are in line with the AgNP peak in Massironi et al. report [11].

As previously mentioned, we have selected the hydrogel film as a wound dressing in this study as it is one of the modern types of a wound dressing with better biocompatibility, biodegradability, and moisture retention characteristics compared to traditional dressings such as gauze. More specifically, for the treatment of second-degree burns with not much exudate, the results of the physical evaluation of the preparation showed a suitable character as a good wound dressing, where the swelling degree and WVTR values indicated that the preparation could adsorb exudate from the wound while maintaining moisture that supports re-epithelialization in the wound area [48]. Another advantage of the hydrogel film preparation is that the film is biodegradable, so it does not cause pain as in traditional wound dressings, which is an important issue because acute wound pain has been shown to increase stress in patients and subsequently negatively affect the quality of life and cause delayed wound healing [48].

Based on particle size and zeta potential results, the hydrogel films showed a good stabilizing effect of ulvan due to the interaction between AgNPs and functional groups in the ulvan structure, which is related to the function of ulvan as a capping agent. With the increase in the number of AgNPs, the tendency of the particles to form agglomerates becomes more extensive, and the surface morphology becomes rougher, indicating more flower-shaped structures as shown in UHF–AgNP1. At lower concentrations of AgNPs, the particles can act as intermolecular connectors, thereby inhibiting the mobility of the polymer chains and enhancing the surface morphology to become smoother and more uniform, as shown in UHF–AgNP0.5.

The size, morphology, stability, and physicochemical properties of the nanoparticles play an important role in their application for wound treatment. A smaller size allows the material to have increased stability and enhanced antimicrobial activity. The smaller the particle size, the wider the surface area. This large surface area will cause the material to become more reactive. The small size allows this material to penetrate the intercellular spaces and increases the affinity of the system due to the increased contact surface area. In this case, AgNP0.5 is easier to penetrate through the bacterial cell wall and then causes damage to its structure than AgNP1. So, the larger the diameter, the weaker the antimicrobial effect. Several studies have found that AgNPs with a size of 20 nm or more are difficult to move into bacterial cells compared to those with a size of 1–15 nm [48,49]. Compared to the other strains, *P. aeruginosa* was more susceptible to AgNPs. Moreover, *P. aeruginosa* (gram-negative bacteria) and *S. aureus* (gram-negative bacteria) are two most common bacteria pathogens to contaminated the wound [42]. The result proved that the UHF-AgNPs dressing had antimicrobial activity on both gram classes of bacteria.

The data from in vivo study showed that wounds treated with UHF–AgNP hydrogel film resulted in faster wound healing based on the percentage of wound closure speed on observation days 5, 7, 14, and 21, namely 19.21%, 35.95%, 91,92%, and 100%. These results indicate a better speed of wound healing than UHF and negative controls, but are not significantly different from positive controls. These results indicate that the condition of the wound treated with a hydrogel film that kept the wound moist for 21 days was better at accelerating healing than the wound with an open condition. Meanwhile, the addition of AgNP to the hydrogel film also significantly accelerated burn healing compared to the hydrogel film without AgNP, this condition was shown as the result of greater wound closure in UHF–AgNP than in UHF. In this case, the antimicrobial mechanism function of AgNPs supported the accelerated healing rate. The mechanism can be explained through the following phenomena: (a) microbial membrane damage, which is caused by the attachment of AgNPs to the cell surface, and subsequently causes structural and functional changes (such as cleft formation, membrane destabilization, membrane piercing, and cytoplasmic leakage); and (b) destruction of sub-cellular structures, caused by the release of Ag ions and subsequent reactive oxygen species (ROS) or inactivation of essential macro-molecules (proteins, enzymes, and nucleotides). However, the most representative mechanisms of AgNPs are adhesion to microbial cells, generation of ROS and free radicals, puncture and penetration of microbial walls within cells, and modulation and modification of microbial signal transduction pathways [27,50,51].

Furthermore, to confirm the healing effect of the second-degree burn AgNP hydrogel film, on the basis of histopathological analysis results (Fig. 6c), on day 21, it was seen that the tissue had undergone complete re-epithelialization and the epidermal structure had intact in UHF, UHF–AgNP, and positive control (triangular sign). However, the microstructure of the regenerated tissue was slightly different where UHF–AgNP showed a denser composition between the epidermis and dermis compared to other samples. In addition, the presence of angiogenesis was also detected in all treatments (arrow-signs). However, this should be further confirmed using immunohistochemical analysis or other relevant methods. Especially in the negative control, it was noticed that there were parts of the epithelial layer that had not undergone partial epithelialization (arrowhead signs) and the number of inflammatory cells was relatively more than in the other samples.

## 5. Conclusion

This study demonstrates that ulvan can be used as a bio-reductant and stabilizer in AgNP synthesis, and successfully used to prepare novel hydrogel film dressing with good antimicrobial capacity. The hydrogel film of UHF-AgNPs possessed a suitable pH, viscosity, swelling degree, and water vapor transmission rate (WVTR). Moreover, the particle size was 13.87–34.77 nm with a potential zeta of

$(-24.5 \pm 1.47) - (-22.43 \pm 2.5)$. UHF–AgNP 0.5 was recommended as the optimum formula based on its physicochemical characterization and antimicrobial activity. In vivo studies on rats showed that UHF-AgNPs significantly improved wound healing compared to negative controls and UHF. This study showed that the application of nanosilver-ulvan for the treatment of second-degree burns was proved to be simple and effective. The antibacterial properties of a combination of AgNPs and ulvan can provide a higher therapeutic potential for wound dressing formulation.

## Author contribution statement

Evi Sulastri, Ahmed Fouad Abdelwahab Mohammed, Khaled M. Elamin: Performed the experiments; Analyzed and interpreted the data; Wrote the paper.

Ronny Lesmana, Muhammad Sulaiman Zubair: Conceived and designed the experiments; Analyzed and interpreted the data.

Nasrul Wathoni: Conceived and designed the experiments; Contributed reagents, materials, analysis tools or data.

## Data availability statement

Data will be made available on request.

## Additional information

No additional information is available for this paper.

## Declaration of competing interest

The authors declare that they have no known competing financial interests or personal relationships that could have appeared to influence the work reported in this paper.

## Acknowledgments

## References

[1] World Health Organization. Burns, Fact Sheet, 2018. Available online: https://www.who.int/news-room/fact-sheets/detail/burns. (Accessed 23 January 2023).

[2] M.J. Hop, S. Polinder, C.H. Van Der Vlies, E. Middelkoop, M.E. Van Baar, Costs of burn care: a systematic review, Wound Repair Regen. 22 (2014) 436–450.

[3] S.Y. Tsai, C.F. Lio, W.C. Yao, C.P. Liu, S.C. Shih, T.Y.T. Wang, K.H. Leong, F.J. Sun, C.F. Kuo, Cost-drivers of medical expenses in burn care management, Burns 46 (2020) 817–824.

[4] T.S. Stashak, E. Farstvedt, A. Othic, Update on wound dressings: indications and best use, Clin. Tech. Equine Pract. 3 (2004) 148–163.

[5] A. Sood, M.S. Granick, N.L. Tomaselli, Wound dressings and comparative effectiveness data, Adv. Wound Care 3 (2014) 511–529.

[6] E. Sulastri, M.S. Zubair, R. Lesmana, N. Wathoni, Development and characterization of ulvan polysaccharides-based hydrogel films for potential wound dressing applications, Drug Des. Dev. Ther. 15 (2021) 4213–4226.

[7] M.I.A. Ibrahim, M.S. Amer, H.A.H. Ibrahim, E.H. Zaghloul, Considerable production of ulvan from Ulva lactuca with special emphasis on its antimicrobial and anti - fouling, Appl. Biochem. Biotechnol. (2022) 1–22.

[8] A. Robic, D. Bertrand, J.F. Sassi, Y. Lerat, M. Lahaye, Determination of the chemical composition of ulvan, a cell wall polysaccharide from Ulva spp. (Ulvales, Chlorophyta) by FT-IR and chemometrics, J. Appl. Phycol. 21 (2009) 451–456.

[9] A. Verma, M.S. Mehata, Controllable synthesis of silver nanoparticles using Neem leaves and their antimicrobial activity, J Radiat Res Appl Sci 9 (2016) 109–115.

[10] M. Behravan, P.A. Hossein, A. Naghizadeh, M. Ziaee, R. Mahdavi, A. Mirzapour, Facile green synthesis of silver nanoparticles using Berberis vulgaris leaf and root aqueous extract and its antibacterial activity, Int. J. Biol. Macromol. 124 (2019) 148–154.

[11] A. Massironi, A. Morelli, L. Grassi, D. Puppi, S. Braccini, G. Maisetta, S. Esin, G. Batoni, C.P. Della, F. Chiellini, Ulvan as novel reducing and stabilizing agent from renewable algal biomass: application to green synthesis of silver nanoparticles, Carbohydr. Polym. 203 (203) (2019) 310–321.

[12] F.R. Diniz, R.C.A.P. Maia, L.R. Andrade, L.N. Andrade, M.V. Chaud, C. Ferreira, C.B. Corrêa, R.L.C. de Albuquerque Junior, L. Pereira da Costa, S.R. Shin, S. Hassan, Silver nanoparticles-composing alginate/gelatine hydrogel improves wound healing in vivo, Nanomaterials 10 (2020) 390.

[13] T. Zia, M. Usman, A. Sabir, M. Shafiq, R.U. Khan, Development of inter-polymeric complex of anionic polysaccharides, alginate/k-carrageenan bio-platform for burn dressing, Int. J. Biol. Macromol. 157 (2020) 83–95.

[14] R. Singla, S. Soni, P. Markand, A. Kumari, In situ functionalized nanobiocomposites dressings of bamboo cellulose nanocrystals and silver nanoparticles for accelerated wound healing, Carbohydr. Polym. 155 (2017) 152–162.

[15] H. Chen, G. Lan, G. Ran, Y. Xiao, K. Yu, B. Lu, A novel wound dressing based on a Konjac glucomannan/silver nanoparticle composite sponge e ff ectively kills bacteria and accelerates wound healing, Carbohydr. Polym. 183 (2018) 70–80.

[16] C. Pansara, R. Mishra, T. Mehta, A. Parikh, S. Garg, Formulation of chitosan stabilized silver nanoparticle-containing wound healing film: in vitro and in vivo characterization, J. Pharmaceut. Sci. 109 (2020) 2196–2205.

[17] A.M. Abdel-Mohsen, J. Jancar, R.M. Abdel-Rahman, L. Vojtek, P. Hyršl, M. Dušková, H. Nejezchlebová, A novel in situ silver/hyaluronan bio-nanocomposite fabrics for wound and chronic ulcer dressing: in vitro and in vivo evaluations, Int. J. Pharm. 520 (2017) 241–253.

[18] E.D. Cavassin, L.F.P. de Figueiredo, J.P. Otoch, M.M. Seckler, R.A. de Oliveira, F.F. Franco, V.S. Marangoni, V. Zucolotto, A.S.S. Levin, S.F. Costa, Comparison of methods to detect the in vitro activity of silver nanoparticles (AgNP) against multidrug resistant bacteria, J. Nanobiotechnol. 13 (2015) 1–16.

[19] M.E. Gondokesumo, O. Wismandanu, T. Hartady, A.M. Rosdianto, H. Goenawan, R. Lesmana, N. Wathoni, U. Supratman, Garcinia mangostana extract enhances skin epithelialization in rat induced burn injury, Pak. Vet. J. 39 (2019) 365–370.

[20] S. Kikionis, E. Ioannou, G. Toskas, V. Roussis, Electrospun biocomposite nanofibers of ulvan/PCL and ulvan/PEO, J. Appl. Polym. Sci. 132 (2015) 1–5.

[21] E. Hernández-Garibay, J.A. Zertuche-González, I. Pacheco-Ruíz, Isolation and chemical characterization of algal polysaccharides from the green seaweed Ulva clathrata (Roth) C. Agardh, J. Appl. Phycol. 23 (2011) 537–542.

[22] N. Wahlström, F. Nylander, E. Malmhäll-Bah, K. Sjövold, U. Edlund, G. Westman, E. Albers, Composition and structure of cell wall ulvans recovered from Ulva spp. along the Swedish west coast, Carbohydr. Polym. 233 (2020) 115852–115861.

[23] H. Tian, X. Yin, Q. Zeng, L. Zhu, J. Chen, Isolation, structure, and surfactant properties of polysaccharides from Ulva lactuca L. from South China Sea, Int. J. Biol. Macromol. 79 (2015) 577–582.

[24] M.A. Khalil, G.M. El Maghraby, F.I. Sonbol, N.G. Allam, P.S. Ateya, S.S. Ali, Enhanced efficacy of some antibiotics in presence of silver nanoparticles against multidrug resistant Pseudomonas aeruginosa recovered from burn wound infections, Front. Microbiol. 12 (2021), 648560.

[25] R. Vinaik, D. Barayan, S. Shahrokhi, M.G. Jeschke, Management and prevention of drug resistant infections in burn patients, Expert Rev. Anti-infect. Ther. 17 (2019) 607–619.

[26] C. Shi, C. Wang, H. Liu, Q. Li, R. Li, Y. Zhang, Y. Liu, Y. Shao, J. Wang, Selection of appropriate wound dressing for various wounds, Front. Bioeng. Biotechnol. 8 (2020) 182.

[27] M.M. Said, M. Rehan, S.M. El-sheikh, M.K. Zahran, M.S. Abdel-aziz, Multifunctional hydroxyapatite/silver nanoparticles/cotton gauze for antimicrobial and biomedical applications, Nanomaterials 11 (2021) 429.

[28] N. Rescignano, R. Hernandez, L.D. Lopez, M. Kenny, C. Mijangos, Preparation of alginate hydrogels containing silver nanoparticles : a facile approach for antibacterial applications, Polym. Int. 65 (2016) 921–926.

[29] L. Zhou, X. Zhao, M. Li, L. Yan, Y. Lu, C. Jiang, Y. Liu, Z. Pan, J. Shi, Antibacterial and wound healing – promoting effect of sponge-like chitosan-loaded silver nanoparticles biosynthesized by iturin, Int. J. Biol. Macromol. 181 (2021) 183–195.

[30] S. Liao, Y. Zhang, X. Pan, F. Zhu, C. Jiang, Q. Liu, Z. Cheng, G. Dai, G. Wu, L. Wang, L. Chen, Antibacterial activity and mechanism of silver nanoparticles against multidrug-resistant Pseudomonas aeruginosa, Int. J. Nanomed. 14 (2019) 1469–1487.

[31] J. Xu, Y. Li, H. Wang, M. Zhu, W. Feng, G. Liang, Enhanced antibacterial and anti-biofilm activities of antimicrobial peptides modified silver nanoparticles, Int. J. Nanomed. 16 (2021) 4831–4846.

[32] A. Alahmad, W.A. Al- zereini, T.J. Hijazin, O.Y. Al-madanat, I. Alghoraibi, O. Al-qaralleh, A. Feldhoff, J.G. Walter, T. Scheper, Green synthesis of silver nanoparticles using Hypericum perforatum L . Aqueous extract with the evaluation of its antibacterial activity against clinical and food pathogens, Pharmaceutics 14 (2022) 1104.

[33] K. Jeeva, M. Thiyagarajan, V. Elangovan, N. Geetha, P. Venkatachalam, Caesalpinia coriaria leaf extracts mediated biosynthesis of metallic silver nanoparticles and their antibacterial activity against clinically isolated pathogens, Ind. Crop. Prod. 52 (2014) 714–720.

[34] F. Fatima, M.F. Aldawsari, M.M. Ahmed, K. Anwer, M. Naz, M.J. Ansari, A.M. Hamad, A. Zafar, M. Jafar, Green synthesized silver nanoparticles using tridax procumbens for topical application: excision wound model and histopathological studies, Pharmaceutics 13 (2021) 1754.

[35] S.J. Yu, Y.G. Yin, J.F. Liu, Silver nanoparticles in the environment, Environ Sci Process Impacts 15 (2013) 78–92.

[36] S. Ahmed, Saifullah, M. Ahmad, B.L. Swami, S. Ikram, Green synthesis of silver nanoparticles using Azadirachta indica aqueous leaf extract, J Radiat Res Appl Sci 9 (2016) 1–7.

[37] K. Jyoti, M. Baunthiyal, A. Singh, Characterization of silver nanoparticles synthesized using Urtica dioica Linn. leaves and their synergistic effects with antibiotics, J Radiat Res Appl Sci 9 (2016) 217–227.

[38] P. Deepak, V. Amutha, C. Kamaraj, G. Balasubramani, D. Aiswarya, P. Perumal, Chemical and Green Synthesis of Nanoparticles and Their Efficacy on Cancer Cells, Elsevier Inc., 2019, pp. 369–387.

[39] A.G. Femi-Adepoju, A.O. Dada, K.O. Otun, A.O. Adepoju, O.P. Fatoba, Green synthesis of silver nanoparticles using terrestrial fern (Gleichenia Pectinata (Willd.) C. Presl.): characterization and antimicrobial studies, Heliyon 5 (2019), e01543.

[40] L. Ran, Y. Zou, J. Cheng, F. Lu, Silver nanoparticles in situ synthesized by polysaccharides from Sanghuangporus sanghuang and composites with chitosan to prepare scaffolds for the regeneration of infected full-thickness skin defects, Int. J. Biol. Macromol. 125 (2019) 392–403.

[41] P. Kanniah, P. Chelliah, J. Reeta, G. Gnanadhas, V. Mahendran, M. Robert, Green synthesis of antibacterial and cytotoxic silver nanoparticles by Piper nigrum seed extract and development of antibacterial silver based chitosan nanocomposite, Int. J. Biol. Macromol. 189 (2021) 18–33.

[42] F. Iram, A. Yasmeen, A. Massey, M.S. Iqbal, S. Asim, M. Irshad, H. Zahid, A.Y. Khan, S.G. Kazimi, Synthesis of gold and silver nanoparticles by use of arabinoglucan from Lallemantia royleana, Int. J. Biol. Macromol. 191 (2021) 1137–1150.

[43] A. Martínez-Higuera, C. Rodríguez-Beas, J.M.A. Villalobos-Noriega, A. Arizmendi-Grijalva, C. Ochoa-Sánchez, E. Larios-Rodríguez, J.M. Martínez-Soto, E. Rodríguez-León, C. Ibarra-Zazueta, R. Mora-Monroy, H.A. Borbón-Nuñez, Hydrogel with silver nanoparticles synthesized by Mimosa tenuiflora for second-degree burns treatment, Sci. Rep. 11 (2021) 1–16.

[44] H.M. Mehwish, G. Liu, M.S.R. Rajoka, H. Cai, J. Zhong, X. Song, L. Xia, M. Wang, R.M. Aadil, M. Inam-Ur-Raheem, Y. Xiong, Therapeutic potential of Moringa oleifera seed polysaccharide embedded silver nanoparticles in wound healing, Int. J. Biol. Macromol. 184 (2021) 144–158.

[45] P. Concórdio-reis, C.V. Pereira, M.P. Batista, C. Sevrin, C. Grand, A.C. Marques, E. Fortunato, F.B. Gaspar, A.A. Matias, F. Freitas, M.A. Reis, Silver nanocomposites based on the bacterial fucose-rich polysaccharide secreted by Enterobacter A47 for wound dressing applications : synthesis, characterization and in vitro bioactivity, Int. J. Biol. Macromol. 163 (2020) 959–969.

[46] M.M.R. Mollick, D. Rana, S.K. Dash, S. Chattopadhyay, B. Bhowmick, D. Maity, D. Mondal, S. Pattanayak, S. Roy, M. Chakraborty, D. Chattopadhyay, Studies on green synthesized silver nanoparticles using Abelmoschus esculentus (L.) pulp extract having anticancer (in vitro) and antimicrobial applications, Arab. J. Chem. 12 (2019) 2572–2584.

[47] S.Z.H. Naqvi, U. Kiran, M.I. Ali, A. Jamal, A. Hameed, S. Ahmed, N. Ali, Combined efficacy of biologically synthesized silver nanoparticles and different antibiotics against multidrug-resistant bacteria, Int. J. Nanomed. 8 (2013) 3187–3195.

[48] C. Shi, C. Wang, H. Liu, Q. Li, R. Li, Y. Zhang, Y. Liu, Y. Shao, J. Wang, Selection of appropriate wound dressing for various wounds, Front. Bioeng. Biotechnol. 8 (2020) 1–17.

[49] A.C. Burduşel, O. Gherasim, A.M. Grumezescu, L. Mogoantă, A. Ficai, E. Andronescu, Biomedical applications of silver nanoparticles: an up-to-date overview, Nanomaterials 8 (2018) 182.

[50] O. Choi, Z. Hu, Size dependent and reactive oxygen species related nanosilver toxicity to nitrifying bacteria, Environ. Sci. Technol. 42 (2008) 4583–4588.

[51] S. Tang, J. Zheng, Antibacterial activity of silver nanoparticles: structural effects, Advanced healthcare materials 7 (2018), 1701503.